ISSN 1070-3284, Russian Journal of Coordination Chemistry, 2021, Vol. 47, No. 11, pp. 780–789. © Pleiades Publishing, Ltd., 2021.

Zinc Complex with Tridentate ONO Schiff Base Ligand: The Characterization and Nanostructure Thereof

M. Saber-Tehrani*

Department of Chemistry, North Tehran Branch, Islamic Azad University, Tehran, 19585-936 Iran

**e-mail: msabertehrani@gmail.com*

Received January 9, 2021; revised March 6, 2021; accepted March 23, 2021

Abstract—A new Zn(II) coordination complex based on the tridentate ONO Schiff base 2-(((2-methoxyphenyl)imino)methyl)phenolate ligand was synthesized and characterized structurally by using FT-IR, ^{1}H NMR, ^{13}C{^{1}H}NMR, UV–Vis and photoluminescence spectroscopies, elemental analysis and single crystal X-ray crystallography (CIF file CCDC no. 2027332). The molecular structure as well as its supramolecular features was studied using structural, Hirshfeld surface analyses as well as computational studies. The supramolecular arrangement of this coordination complex is directed by a series of hydrogen bonding interactions, including O–H···O, C–H···Br and C–H···π. The C–H···π energies in this compound calculated to be in the range of 5.79–7.99 Å. The compound is also successfully synthesized in three different concentrations by ultrasonic irradiation. The product was characterized by different techniques and the morphology was analyzed using field-emission scanning electron microscopy. The comparison between samples synthesized using ultrasonic irradiation demonstrated that lower concentrations of initial reagents decreased plate size and increased the homogenization of particle size distribution.

Keywords: Zn(II) coordination complex, tridentate ligand, Schiff base, C–H···π-interactions

DOI: 10.1134/S107032842111004X

INTRODUCTION

In the last decades, the design and synthesis of zinc(II) coordination complexes have received much attention because of their potential applications as metalloenzyme mimicry, molecular sensor and catalyst [1–5]. Zinc is the second most abundant 3*d* metal ion in the human body and plays several crucial roles in a variety of biological processes [6]. Zn(II) ion with a filled d^{10} configuration is colorless, diamagnetic and usually does not involve in redox reactions. Because of the lack of ligand field stabilization energy, the Zn(II) cation exhibits high flexibility concerning the coordination geometry and the most common coordination numbers are 4, 5, and 6 [7, 8]. Also, Zn^{2+} has an intermediate hard/soft acid character, which allows it to be coordinated by ligands containing hard and soft donors such as nitrogen, oxygen, and sulfur. Multidentate ligands containing heteroatoms play a remarkable role in coordination chemistry because of their potential to encapsulate metal ions and thus control the geometry of complexes to form discrete coordination compounds [9–11]. Multidentate Schiff base ligands have been widely investigated in coordination chemistry mainly because of their facile synthesis, ease of functionalization, biocompatibility, and their ability to form stable metal complexes with a large number of transition metal ions [8, 12, 13]. Following these research strategies and for investigating the solid-state chemistry of group IIB metal coordination complexes [14–18], a new Zn(II) coordination complex based on tridentate ONO Schiff base 2-(((2-methoxyphenyl)imino)methyl)phenolate (L) ligand was synthesized and characterized using spectroscopic techniques and single-crystal X-ray crystallography (Scheme 1). The supramolecular structure of this compound is investigated using structural and Hirshfeld surface analyses as well as computational studies. It is also of our interest to evaluate the self-assembly of this complex in the nanoscale realm. Recent advances in nanostructured materials have been led by developing new synthetic methods that provide control over size, morphology, and nano/microstructure. The utilization of high-intensity ultrasound offers a facile, versatile synthetic tool for nanostructured materials such as nanocoordination compounds [19–21]. In this regard, the [ZnLBr(CH_3OH)] (**I**) was synthesized in different concentrations through ultrasonic irradiation. The fabricated complex was fully characterized, and the effect of the reagent's initial concentrations was investigated. Schematic representation of coordination compound **I** is shown below:

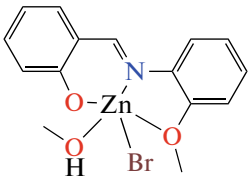

Scheme 1.

EXPERIMENTAL

Apparatus and reagents. *o*-Anisidine, salicylaldehyde and $ZnBr_2$ for the synthesis of 2-(((2-methoxyphenyl)imino)methyl) phenolate (LH) ligand and [ZnLBr(CH_3OH)] (**I**), respectivily, were purchased from Aldrich Chemical Company Inc. The Fourier transform infrared spectroscopy was performed on a Nicolet 100 Fourier Transform IR spectrometer in the 4000–500 cm^{-1} range using KBr disk technique. Elemental analyses (carbon, hydrogen, and nitrogen) were performed on a Costech ECS 4010 CHN-O. An Electrothermal 9100 apparatus was used for melting points measurement. NMR spectra were recorded on a Bruker AC-300 spectrometer for protons at 300.13 MHz and for $^{13}C\{^1H\}$ at 75.45 MHz. UV–Vis spectra were recorded on a Perkin Elmer, Lambada 35 spectrometer in MeOH at 25°C, and luminescence spectrum were performed using a Perkin Elmer LS 55 spectrophotometer.

Single crystal X-ray diffraction. X-ray diffraction data was collected at 100(1) K on Bruker APEX-II four-circle diffractometer with graphite-monochromated MoK_α radiation ($\lambda = 0.71069$ Å) [22]. The data were corrected for Lorentz-polarization as well as for absorption effects [23]. Precise unit-cell parameters were determined by a least-squares fit reflections of the highest intensity, chosen from the whole experiment. The structure was solved with SHELXT-2014 [24] and refined with the full-matrix least-squares procedure on F^2 by SHELXL-2014 [25]. All non-hydrogen atoms were refined anisotropically, hydrogen atoms were placed in idealized positions and refined as 'riding model' with isotropic displacement parameters set at 1.2 (1.5 for hydroxyl groups) times U_{eq} of appropriate carrier atoms. The crystal data obtained from single crystal X-ray crystallography is listed in Table 1. Hirshfeld surface analysis was carried out using Crystal Explorer 3.1 software [26].

Supplementary material for structure **I** has been deposited with the Cambridge Crystallographic Data Centre (CCDC no. 2027332; deposit@ccdc.cam.ac.uk or http://www.ccdc.cam.ac.uk).

Computational methods. Density functional theory (DFT) and time-dependent density functional theory (TD-DFT) calculations of the intermolecular interactions were performed using the ORCA quantum chemistry suite [27]. The BLYP exchange-correlation functional [27] with the D3 empirical dispersion correction (BLYP-D3) was employed to calculate the intermolecular interaction energies between two relative fragments [28]. It has been found out that small BSSE effects are absorbed by the D3 empirical potential. Thus, the basis set superposition error (BSSE) is not taken into account [29]. To calculate the intermolecular interaction binding energies in the solid-state, the solid-state coordinates obtained from X-ray crystallography were used. This procedure and this level of theoretical calculation have been successfully used to explore similar intermolecular interactions in the solid-state [30, 31]. An all-electron triple-zeta basis-set with two polarization functions, TZ2P, has been employed to describe all the atoms, while using frozen core approximation. The zeroth-order regular approximation (ZORA) was employed for considering the relativistic effect.

Synthesys of 2-(((2-methoxyphenyl)imino)methyl)phenol (LH) was carried out by the condensation of *o*-anisidine with salicylaldehyde in refluxed anhydrous ethanol with 80% yield according to the reported procedure [32].

FT-IR (KBr; ν, cm^{-1}): 3445 w, broad, 3061w, 3012 w, 2968 w, 2835 w,1615 s, 1588 s, 1569 s, 1483 s, 1246 s, 849 m, 792 s. ^1H NMR ($CDCl_3$; δ, ppm): 3.88 (s., 3H, $-OCH_3$), 6.88–7.02 (m., 4H, H_{Ar}), 7.21–7.28 (m., 2H, H_{Ar}), 7.32–7.40 (m., 2H, H_{Ar}), 8.72 (s., 1H, −N=CH−) and 13.88 (s., 1H, −OH). $^{13}C\{^1H\}$NMR ($CDCl_3$; δ, ppm): 56.9, 111.5, 114.2, 120.8, 121.7, 122.6, 123.1, 126.6, 134.9, 135.7, 142.6, 152.8, 167.3, 167.8. UV–Vis: λ_{max}(CH_3OH, nm): 282, 346 and 450 (broad peak).

Synthesys of (methanol)[2-(((2-methoxyphenyl)imino)methyl)phenol]dibromidozinc(II) (I, $C_{15}H_{16}NO_3BrZn$). In the presence of potassium hydroxide, the reaction of LH with $ZnBr_2$ in methanol resulted in deprotonation of the ligand at the hydroxyl group to form [ZnLBr(CH_3OH)] (**I**) (Scheme 1). To a solution of 0.1 mmol $ZnBr_2$ in 5 cm^3 methanol, a solution of LH (0.1 mmol) and KOH (0.1 mmol) in 5 cm^3 of methanol was added with stirring. The mixture was heated at 50°C for about 15 min, resulting in the immediate formation of a light greenish-yellow transparent solution. Bright yellow single crystals suitable for X-ray crystallography were obtained upon slow evaporation of the solution within a week (yield was 72%).

For $C_{15}H_{16}NO_3BrZn$			
Anal. calcd., %	C, 44.64	H, 4.00	N, 3.47
Found, %	C, 44.62	H, 3.96	N, 3.45

FT-IR (KBr; ν, cm^{-1}): 3435 m, 3045 w, 2930 w, 2837 w, 1677 s, 1637 s, 1610 s, 1534 s, 1255 s, 1148 s, 842 m, 743 s. ^1H NMR (CD_3OD; δ, ppm): 3.85 (s., 3H, $-OCH_3$), 6.92–7.06 (m., 4H, H_{Ar}), 7.25–7.33

Table 1. Crystallographic data and structure refinement for complex **I**

Parameter	Value
Empirical-formula	$C_{15}H_{16}NO_3BrZn$
Mr	403.57
T, K	100(1)
Crystal system	Monoclinic
Space group	$P2_1/n$
a, Å	7.7841(2)
b, Å	16.6751(5)
c, Å	12.2281(3)
α, deg	90
β, deg	101.986(1)
γ, deg	90
Volume, Å^3	1552.61(7)
Z	4
ρ_{calcd}, mg/m^3	1.727
μ, mm^{-1}	4.163
F(000)	808.839
2θ, deg	67.68
Reflections collected/unique	192307/7192
R_{int}	0.0595
Reflections with $I > 2\sigma(I)$	5633
GOOF	1.1735
R_1[a] ($I > 2\sigma(I)$)	0.0292
wR_2[b] ($I > 2\sigma(I)$)	0.0533
Largest diff. peak and hole, e Å^{-3}	0.7622 and −0.6714

[a] $R_1 = \Sigma||F_o| - |F_c||/\Sigma|F_o|$; [b] $wR_2 = [\Sigma(w(F_o^2 - F_c^2)^2)/\Sigma w(F_o^2)2]^{1/2}$.

(m., 2H, H_{Ar}), 7.37–7.45 (m., 2H, H_{Ar}) and 8.76 (s., 1H, –N=CH–). $^{13}C\{^1H\}$NMR (CD_3OD; δ, ppm): 57.1, 111.7, 114.5, 121.0, 121.9, 122.8, 123.2, 126.7, 135.1, 135.9, 142.8, 153.1, 167.6, 168.0. UV–Vis: λ(CH_3OH; λ, nm): 236, 286, 325 and 401 nm; m.p.: 233–235°C.

Synthesis of nanostructured [Zn(L)Br(CH_3OH)] (I) was carried out by using ultrasonic irradiation according to the below-described procedure. In a round bottom flask which was fixed in the bath of the ultrasonic generator operating at 40 kHz with a maximum power output of 305 W, 5 cm^3 of $ZnBr_2$ (0.1 mmol) methanolic solution was positioned (25 cm^3). Into this solution, a 5 cm^3 methanolic solution of the LH ligand (0.1 mmol) along with the KOH (0.1 mmol) was added dropwise. Ultrasonic irradiation was applied for 15 min; the solid product was filtered off, washed with a small amount of cold methanol and dried in air at room temperature. To study the effect of reagent's initial concentrations on the size and morphology of nanostructured [ZnLBr(CH_3OH)], the described procedure was carried out with 0.1, 0.05, and 0.03 mol L^{-1} concentrations (yield was 88%).

For $C_{15}H_{16}NO_3BrZn$

Anal. calcd., %	C, 44.64	H, 4.00	N, 3.47
Found, %	C, 44.60	H, 3.98	N, 3.48

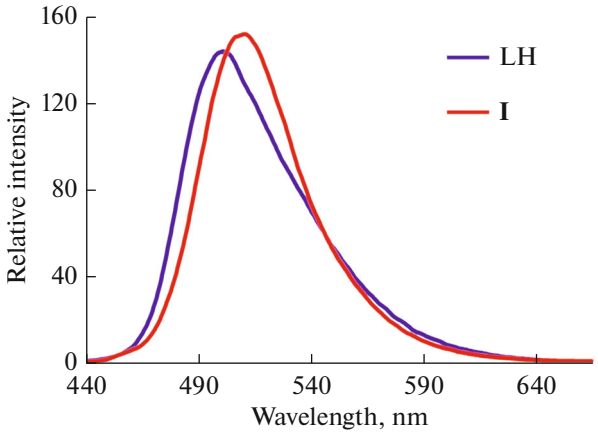

Fig. 1. Fluorescence spectra of 2-(((2-methoxyphenyl)imino)methyl)phenol (LH) (6.1×10^{-4} M) ligand and complex **I** (6.2×10^{-4} M) at λ_{ex} = 410 nm, in CH_3OH at room temperature.

FT-IR (KBr; ν, cm^{-1}): 3433 m, 3042 w, 2930 w, 2835 w, 1677 s, 1637 s, 1609 s, 1533 s, 1255 s, 1148 s, 842 m, 744 s.; m.p.: 233–235°C.

RESULTS AND DISCUSSION

Schiff base ligands can be synthesized easily and generate stable coordination complexes with various metal ions [33, 34]. A survey in Cambridge Structural Database (CSD) revealed that 2-(((2-methoxyphenyl)imino)methyl)phenol (LH) ligand has been previously used for the formation of number of coordination complexes [35–40]. The LH ligand can exist in different tautomeric forms and can switch between the enol and keto forms [41, 42]. [ZnLBr(CH_3OH)] (**I**) was synthesized by reacting $ZnBr_2$ with LH ligand in basic methanolic solution. This compound was structurally characterized by using elemental analysis, FT-IR, ^{1}H NMR, $^{13}C\{^1H\}$NMR, UV–Vis, X-ray crystallography and photoluminescence spectroscopies. The FT-IR characteristic frequencies of compound **I** and the free LH ligand are listed in the experimental section. In the FT-IR spectroscopy, the ν(C=N) stretching frequencies of **I** and LH are observed at 1610 and 1615 cm^{-1}, respectively. The stretching frequencies of C–O in **I** and LH are seen at 1255 and 1246 cm^{-1}, respectively. The C–H stretching and bending frequencies of the methyl group in **I** are appeared at 2837 and 1475 cm^{-1}, respectively. The stretching frequencies of the terminal M–X and M–O moieties are located in the far IR-spectrum, at lower frequencies than could be assigned here. The characteristic features in the absorbance spectrum of Zn complex remain similar to that of free LH ligand, which can be assigned to π–π* and *n*–π* transition belongs to the free LH ligand, according to the TD-DFT calculation (Fig. S1). The bands between the 200–400 nm in the predicted electronic spectrum are assigned to the electronic transitions from the HOMO-3, HOMO-2, HOMO-1 and HOMO molecular orbitals to LUMO of free LH ligand. The ^{1}H NMR and $^{13}C\{^1H\}$NMR data for free LH ligand and complex **I** are shown in the experimental section. A comparison between the ^{1}H NMR spectra of the title complex and its free ligand clearly indicated that the signal of the –OH proton (13.88 ppm) in the spectrum of the free LH ligand is absent in the spectrum of complex **I**, indicating the removal of the –OH proton and the formation of Zn–O bonds. Furthermore, the $^{13}C\{^1H\}$NMR spectra of free LH ligand and complex **I** showed a singlet at around 56.8 ppm for $-CH_3$ group and thirteen singlets at 111–168 ppm for the aromatic carbon atoms and imine carbon atom. The photoluminescence spectra of free LH ligand and complex **I** is shown in Fig. 1. As shown in Fig. 1, the maximum emission wavelength in the fluorescence spectra of free LH ligand and complex **I** is located at 510 and 520 nm upon excitation at 401 nm, respectively. Also, the shapes of the fluorescence spectra of the free LH ligand and complex **I** are similar. Therefore, the fluorescence properties of complex **I** are due to the π* → π or π* → *n* transitions in coordinated LH [15, 17, 43, 44]. The elemental analysis reveals that the synthesized complex of the proposed structure in the 1 : 1 metal : ligand stoichiometry, which is further supported by the X-ray analysis.

X-ray crystallography reveals that **I** crystallizes in the monoclinic $P2_1/n$ space group. The ORTEP draw of the zinc coordination complex, drawn at a 50% ellipsoid probability level is shown in Fig. 2. Some selected bond distances and angles are collected in Table 2. The asymmetric unit contains a crystallographically independent L ligand, a Zn(II) ion, a bromide ion and a coordinated methanol molecule. The molecular structure of this compound reveals that the five-coordinate zinc ion is coordinated by tridentate (ONO) Schiff base ligand, a bromide ion and coordinating methanol molecule. The index of trigonality (τ_5), as defined by Addison and Reedijk [45], is 0.55 for Zn(II) ion which implies that the coordination environment around the metal center can be described as an intermediate between square-pyramidal and trigonal pyramidal formed by the methoxy (O(1)) and phenolate (O(2)) oxygen atoms, imine nitrogen atom, terminal bromide ion and the oxygen atom (O(3)) of methanol (Table 2). All the bond distances and angles are in the expected range. The dihedral angle between the planes of two substituted phenyl rings of L ligand is 32.10°. The defined dihedral ligand for the ligand L lies between 16.44° (Ref. code: COSALA) to 44.48° (Ref. code: EJIYUR) in the crystal structures of reported coordination complexes. Hence the ligand can adjust in conformation to fit the requirement of coordination environment of the metal center and the

optimal interatomic close contacts distances in the 3D structure [46, 47].

The crystal packing analysis of this compound reveals that discrete [ZnLBr(CH_3OH)] (**I**) complexes are connected via $R_2^2(8)$ O–H···O and C–H···Br hydrogen bonds in the crystallographic *bc*-plane (Table 3 and Fig. 3). Several C–H···π interactions, with CH···aromatic centroid distances ranging from 2.783(2) to 3.466(1) Å, between aromatic hydrogen atoms or hydrogen atoms of pendant CH_3 group and aryl ring, forming the three-dimensional crystal packing (Table 3 and Fig. 4). It is to be mentioned that the aryl rings of neighboring L ligands are not parallel and no π–π interactions exist in the crystal structure of the zinc complex.

The Hirshfeld surface analysis was carried out to analyze the strength and role of the intermolecular interactions in the crystal structure of coordination compound [ZnLBr(CH_3OH)] (**I**). The Hirshfeld surface analysis was developed for quantifying the intermolecular interactions involved in the crystal structure [48]. A pie-chart of percentage contributions of different intermolecular interactions and the two-dimensional fingerprint plots of the complex **I** indicate different non-covalent interactions and are shown in Figs. 5, S2, S3, and Table S1. The data reveals that the crystal structure of the zinc(II) coordination compound is directed by H···H, C–H···π, C–H···Br, C–H···O and O–H···O interactions. The H···H and C–H···π interactions are the most abundant non-covalent interactions and play a crucial role in driving the crystal structure of **I** and C–H···Br, C–H···O and C/O–H···O interactions are the next priorities, respectively. It has been shown that the large percentage values for the weak van der Waals H···H interactions is typical for organic molecules and is consistent with the presence of CH groups in the L ligand backbone, OCH_3 pendant group and coordinating methanol molecule [49, 50].

The shape index (–1.0 (red) and +1.0 (blue)) and curvedness between –4.0 (red) and +0.4 (blue) of Hirshfeld surface of zinc complex is shown in Fig. S2. The shape index plot of the coordination compound showed a large red depression in the surface above the aromatic ring of concave curvature, which is attributed to the C–H···π interactions, while C–H donor regions have the opposite curvature. The negligible role of π···π stacking interactions in the crystal packing of this compound can be anticipated due to the lack of a large flat green surface on the curvedness surface indicates. The O–H···O hydrogen bonding interaction, presented by a large bright red spot on the Hirshfeld surface, appears as a characteristic pair of sharp spikes with the upper spike (de > di) and the lower spike (de < di) corresponds to the hydrogen-bond donor and the hydrogen-bond acceptor, respectively.

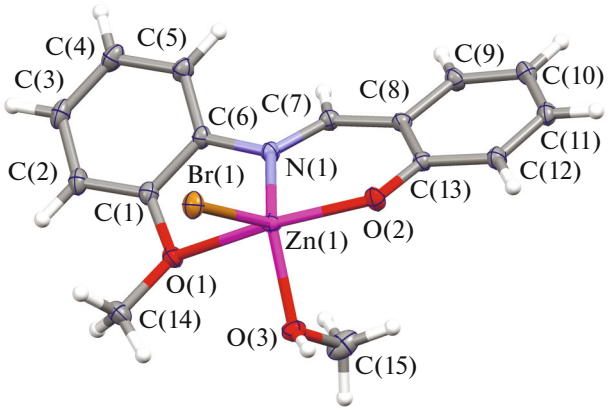

Fig. 2. ORTEP diagram of compound **I** drawn at 50% probability ellipsoids.

The computational calculation is carried out to analyze the strength of intermolecular interactions that govern the crystal structure of the zinc-coordination compound. The interaction binding energies, obtained from the BLYP-D3 calculation on two fragments, help us to evaluate the strength of the intermolecular interactions between discrete molecular complexes (Table 3). The geometry of the selected fragments was obtained directly from the crystallographic

Table 2. Selected bond distances (Å) and angles (deg) for **I**

Bond	*d*, Å
Zn(1)–O(1)	2.446(1)
Zn(1)–O(2)	1.992(1)
Zn(1)–O(3)	2.022(1)
Zn(1)–N(1)	2.025(1)
Zn(1)–Br(1)	2.3455(1)
Angle	**ω, deg**
O(1)Zn(1)O(2)	153.79(4)
O(1)Zn(1)O(3)	78.50(4)
O(2)Zn(1)O(3)	93.58(2)
N(1)Zn(1)O(1)	70.70(5)
N(1)Zn(1)O(2)	92.49(5)
N(1)Zn(1)O(3)	119.40(5)
N(1)Zn(1)Br(1)	120.41(4)
O(1)Zn(1)Br(1)	94.93(3)
O(2)Zn(1)Br(1)	111.09(3)
O(3)Zn(1)Br(1)	112.95(4)

Table 3. Selected hydrogen bond and C–H···π geometries for coordination compound **I**

D–H···A	Distance, Å			Angle D–H···A, deg	Binding energy, kcal/mol	Sym. Code
	D–H	H···A	D···A			
C(2)–H(2)···Br(1)	0.950(3)	2.976(2)	3.796(2)	145.3(2)	–12.54	$1-x, 1-y, 2-z$
C(15)–H(15A)···Br(1)	0.98(1)	3.089(9)	3.854(2)	135.9(8)	–180.78	$1-x, 1-y, 1-z$
O(3)–H(3)···O(2)	0.80(2)	1.80(2)	2.599(2)	178.0(3)		$1-x, 1-y, 1-z$
C–H···π	D–H	$H\cdots\pi_{centroid}$	D···A	Angle D–H···A, deg	Binding energy, kcal/mol	Sym. Code
$C(5)–H(5)\cdots\pi_{C(8)–C(13)}$	0.950(2)	3.322(1)	3.779(2)	111.75(1)	–6.04	$1/2+x, 1/2-y, 1/2+z$
$C(10)–H(10)\cdots\pi_{C(1)–C(6)}$	0.950(2)	2.783(2)	3.575(1)	141.36(1)	–7.99	$1/2+x, 1/2-y, -1/2+z$
$C(14)–H(14C)\cdots\pi_{C(8)–(13)}$	0.980(8)	3.466(1)	3.926(1)	111.12(2)	–5.79	$1.5-x, 1/2+y, 1.5-z$

information file (CIF) and is shown in Fig. S4. The calculated binding energies of intermolecular interactions in this complex are in the range of those found for neutral complexes [51–53]. The C–H···π interaction energies in [ZnLBr(CH_3OH)] calculated to be in the range of 5.79–7.99, which is in agreement with the reported values for C–H···π and C–H···X (X = Cl, Br, I) non-classical hydrogen bonds (Table 3) [54–57]. Notably, the head-to-tail dimeric fragments interaction energies containing two O–H···O and two C–H···Br hydrogen bonding interactions are much larger than that of the fragments in which only a single C–H···Br interaction is involve (Table 3, Fig. S4). The dimer interaction energy value is comparable to the reported values [58, 59].

The Zn(II) coordination compound was prepared in methanol by ultrasonic irradiation according to the procedure described in the experimental section. The final products were characterized by powder X-ray diffraction (PXRD), FT-IR spectroscopy and elemental analysis. The FT-IR spectrums as well as the elemental analysis of the samples synthesized by both the conventional and the sonochemical methods, are indistinguishable. The morphological characteristics of the synthesized complex using the sonochemical method were studied by field-emission scanning electron microscopy (FE-SEM). Figure 6 shows the FE-SEM micrographs of the nanoplates of zinc-complex synthesized by the ultrasonic generator, with 305 W ultrasonic power, in the reagent initial concentration of 0.03, 0.05, and 0.1 mol L^{-1} for 15 min. The FE-SEM images of this compound show plate morphology with diameters ranging from nano- to micro-scale. Our results reveal that lower concentrations of initial reagents resulted in the formation of a plate with decreased sizes and also an increase in the uniformity and the homogenization of particle size distribution. Therefore, nanoplates synthesized by using higher concentrations of starting materials are larger in size

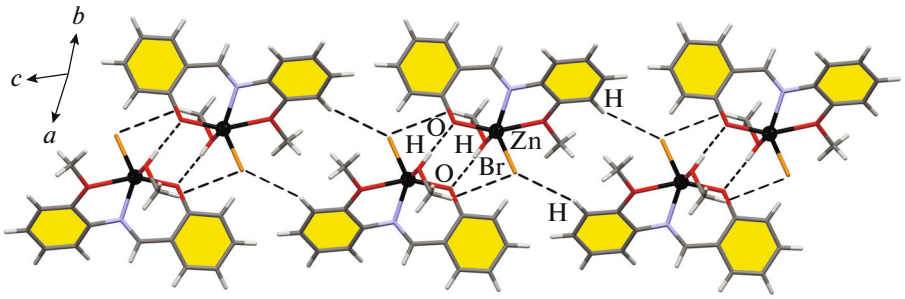

Fig. 3. Representation of the crystal packing of **I** showing the association of discrete molecular units via $R_2^2(8)$ O–H···O and C–H···Br hydrogen bonds in the crystallographic *bc*-plane.

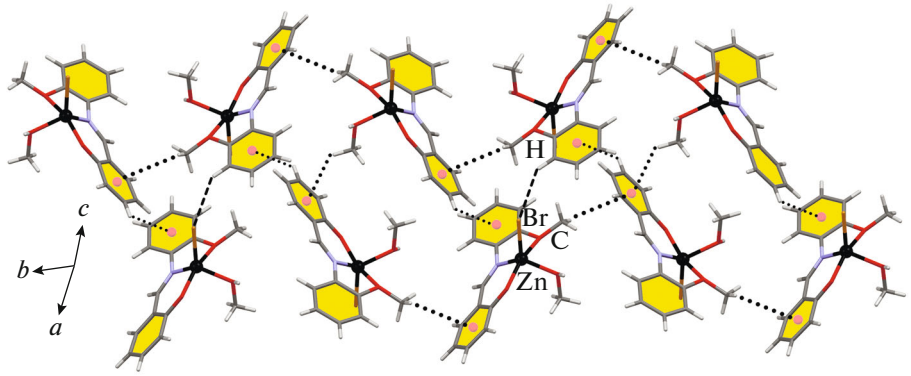

Fig. 4. Representation of the crystal packing of [ZnLBr(CH_3OH)] (**I**) showing the supramolecular association of molecular units via C–H···π interactions between aromatic hydrogen atoms or hydrogen atoms of pendant CH_3 group and aryl ring, forming the three-dimensional crystal packing.

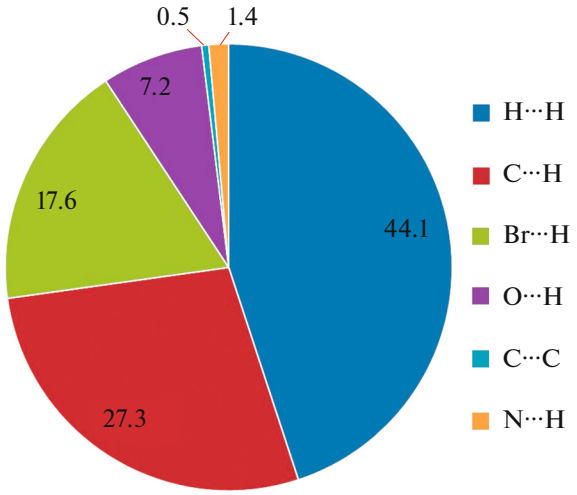

Fig. 5. Pie-chart showing the relative contributions of different intermolecular interactions to the Hirshfeld surface area of compound **I**.

than those produced using lower concentrations (Fig. 6).

Figure 7 shows the simulated XRD pattern from single-crystal X-ray data of the complex **I** in comparison with the XRD pattern of a typical sample synthesized by the ultrasonic irradiation. All the X-ray diffraction peaks can be well-indexed to a known bulk phase, and the peak positions remain unchanged compared with the simulated and experimental powder X-ray diffraction patterns. The results revealed that the size of the coordination complex is related to the starting materials concentrations and can be controlled using ultrasonic irradiation.

A new Zn(II) coordination complex with tridentate ONO Schiff base 2-(((2-methoxyphenyl)imino)methyl)phenolate ligand was synthesized and characterized using FT-IR, ^{1}H NMR, ^{13}C{^{1}H}NMR, UV–Vis and photoluminescence spectroscopies, elemental analysis and X-ray crystallography. The crystal packing of the zinc coordination compound was investigated using structural, Hirshfeld surface analyses and computational calculations. The crystal packing analysis reveals that the crystal structure is constructed via a series of O–H···O, C–H···Br and C–H···π hydrogen bonding interactions. This complex is also synthesized using ultrasonic irradiation and the role of initial reagent concentrations on the size and morphology of the nanostructured compound. Results of this study might be of interest to those who are studying the solid-state and the nanochemistry of Zn(II) containing chelating Schiff base ligand.

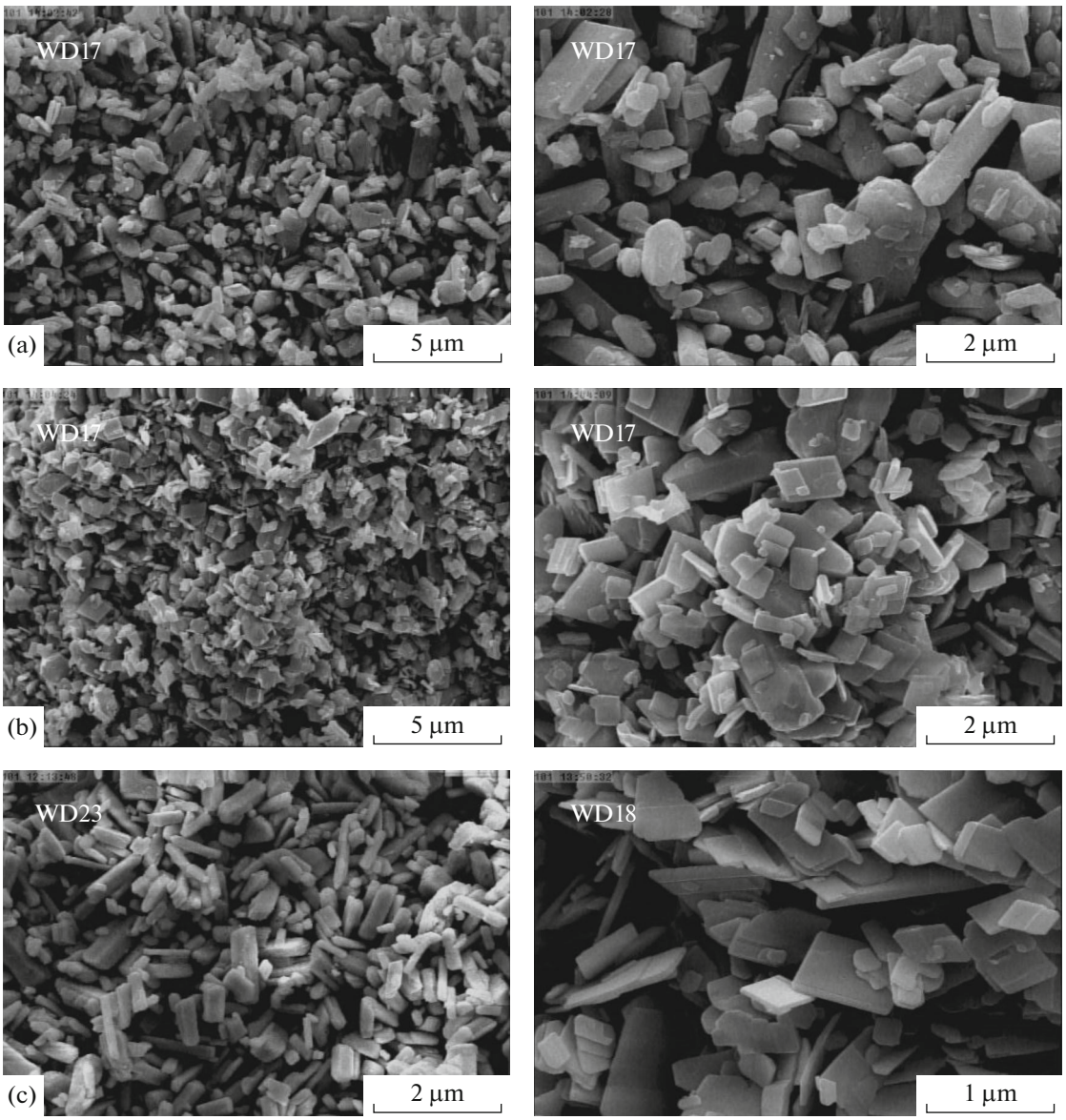

Fig. 6. FE-SEM images of complex **I** prepared using ultrasonic generator 305 W. 0.1 M (a) 0.05 (b) and 0.03 M.

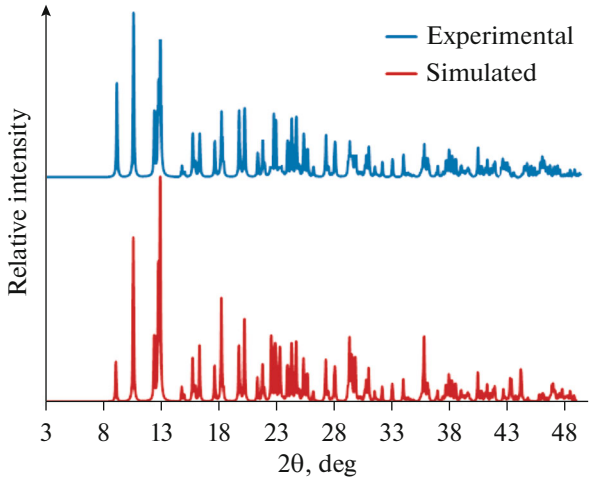

Fig. 7. A comparison between simulated PXRD pattern (red) and the PXRD pattern of nanostructured **I** synthesized by ultrasonic irradiation (blue).

ACKNOWLEDGMENTS

The work was supported by the Department of Chemistry, North Tehran Branch, Islamic Azad University in Tehran, Iran.

SUPPLEMENTARY MATERIALS

The online version contains supplementary material available at https://doi.org/10.1134/S107032842111004X.

REFERENCES

1. Sarkar, A., Ghosh, A.K., Bertolasi, V., and Ray, D., *Dalton Trans.*, 2012, vol. 41, p. 1889.
2. Zhang, C., Che, Y., Zhang, Z., et al., *Chem. Commun.*, 2011, vol. 47, p. 2336.
3. Hirano, T., Kikuchi, K., Urano, Y., et al., *J. Am. Chem. Soc.*, 2000, vol. 122, p. 12399.
4. Dai, Z. and Canary, J.W., *New J. Chem.*, 2007, vol. 31, p. 1708.
5. Kaler, S., McKeown, P., Ward, B.D., and Jones, M.D., *Inorg. Chem. Front.*, 2021, vol. 8, p. 711.
6. Vahrenkamp, H., *Dalton Trans.*, 2007, p. 4751.
7. Wöckel, S., Gałęzowska, J., Dechert, S., et al., *Eur. J. Inorg. Chem.*, 2012, p. 4728.
8. Matos, C.P., Addis, Y., Nunes, P., et al., *J. Inorg. Biochem.*, 2019, vol. 198, p. 110727.
9. Benaissa, H., Wolff, M., Robeyns, K., et al., *Cryst. Growth Des.*, 2019, vol. 19, p. 5292.
10. Burlov, A.S., Uraev, A.I., and Ikorskii, V.N., *Russ. J. Ener. Chem.*, 2008, vol. 78, p. 1230.
11. Garnovskii, A., Burlov, A., and Lysenko, K., *Russ. J. Coord. Chem.*, 2009, vol. 35, p. 120.
12. Blackman, A.G., *Eur. J. Inorg. Chem.*, 2008, p. 2633.
13. Porchia, M., Pellei, M., Bello, F.D., and Santini, C., *Molecules*, 2020, vol. 25, p. 5814.
14. Liu, Y.Y., Wang, Z.H., Yang, J., et al., *CrystEngComm.*, 2011, vol. 13, p. 3811.
15. Ostad, S.N., Abedi, A., Amani, V, et al., *J. Iran. Chem. Soc.*, 2016, vol. 13, p. 1417.
16. Amani, V., Ahmadi, R., Naseh, M., and Ebadi, A., *J. Iran. Chem. Soc.*, 2017, vol. 14, p. 635.
17. Amani, V., *J. Mol. Struct.*, 2018, vol. 1155, p. 477.
18. Saghatforoush, L., Moeini, K., Golsanamlou, V., et al., *Z. Inorg. Chim. Acta*, 2018, vol. 483, p. 392.
19. Safarifard, V. and Morsali, A., *Coord. Chem. Rev.*, 2015, vol. 292, p. 1.
20. Esrafili, L., Tehrani, A.A., and Morsali, A., *Ultrason. Sonochem.*, 2017, vol. 39, p. 307.
21. Paqhaleh, D.M.S., Hashemi, L., Amani, V., et al., *Inorg. Chim. Acta*, 2013, vol. 407, p. 1.
22. *CrysAlisPro*, Yarnton England, 2009.
23. *CPVD Agilent Technologies*, Agilent Technologies Ltd., 2011.
24. Sheldrick, G.M., *Acta Crystallogr., Sect. A: Found. Adv.*, 2015, vol. 71, p. 3.
25. Sheldrick, G.M., *Acta Crystallogr., Sect. C: Struct. Chem.*, 2015, vol. 71, p. 3.
26. Neese, F., Wennmohs, F., Becker, U., et al., *AORCA, version 3.0*, Mülheim/Ruhr: Max Planck Institute for Chemical Energy Conversion, 2014.
27. Becke, A.D., *Phys. Rev., A*, 1988, vol. 38, p. 3098.
28. Grimme, S., Antony, J., Ehrlich, S., and Krieg, H., *J. Chem. Phys.*, 2010, vol. 132, p. 154104.
29. Guerra, C.F., Zijlstra, H., Paragi, G., and Bickelhaupt, F.M., *Chem. A. Eur. J.*, 2011, vol. 17, p. 12612.
30. Tehrani, A.A., Ghasempour, H., Morsali, A., et al., *CrystEngComm.*, 2017, vol. 19, p. 1974.
31. Chakraborty, P., Purkait, S., Mondal, S., et al., *CrystEngComm.*, 2015, vol. 17, p. 4680.
32. Wu, J.Q., Pan, L., Li, Y.G., et al., *Organomet.*, 2009, vol. 28, p. 1817.
33. Arulmurugan, S., Kavitha, H.P., and Venkatraman, B., *Rasayan. J. Chem.*, 2010, vol. 3, p. 385.
34. Raman, N., Raja, S.J., and Sakthivel, A.J., *Coord. Chem.*, 2009, vol. 62, p. 691.
35. Chen, Q., Huang, J., and Yu, J., *Inorg. Chem. Commun.*, 2005, vol. 8, p. 444.
36. Chen, Q., *J. Appl. Organomet. Chem.*, 2006, vol. 20, p. 758.
37. Reddy, P.A., Nethaji, M., and Chakravarty, A.R., *Inorg. Chem. Commun.*, 2003, vol. 6, p. 698.
38. Charland, J., Gabe, E., Khoo, L., and Smith, F., *Polyhedron*, 1989, vol. 8, p. 1897.
39. Yousaf, M., Liu, Q., Huang, J., et al., *Inorg. Chem. Commun.*, 2000, vol. 3, p. 105.
40. Lu, W.Y., Hsiao, M.W., Hsu, S.C., et al., *Dalton Trans.*, 2012, vol. 41, p. 3659.
41. Hajiashrafi, T., Zekriazadeh, R., Flanagan, K.J., et al., *Acta Crystallogr., Sect. C: Struct. Chem.*, 2019, vol. 75, p. 178.
42. Hoshino, N., Inabe, T., Mitani, T., and Maruyama, Y., *Bull. Chem. Soc. Jpn.*, 1988, vol. 61, p. 4207.
43. Taheriha, M., Ghadermazi, M., and Amani, V., *J. Mol. Struct.*, 2016, vol. 1107, p. 57.
44. Choopani Jouybaria, H., Alizadeha, R., Banisaeeda, H., and Amani, V., *Inorg. Chim. Acta*, 2020, vol. 506, p. 119553.
45. Addison, A.W., Rao, T.N., Reedijk, J., et al., *Dalton Trans.*, 1984, p. 1349.
46. Lakshmi, S., Geetha, K., Mahalingam, M.G., and Shanmugam, G., *J. Chem. Sci.*, 2016, vol. 128, p. 1095.
47. Reddy, P.A., Nethaji, M., and Chakravarty, A.R., *Eur. J. Inorg. Chem.*, 2004, p. 1440.
48. Spackman, M.A. and Jayatilaka, D., *CrystEngComm.*, 2009, vol. 11, p. 19.
49. McKinnon, J.J., Spackman, M.A., and Mitchell, A.S., *Acta Crystallogr., Sect. B:, Struct. Sci.*, 2004, vol. 60, p. 627.
50. Spackman, M.A. and McKinnon, J.J., *CrystEngComm.*, 2002, vol. 4, p. 378.

51. Sadhukhan, D., Maiti, M., Pilet, G., et al., *Eur. J. Inorg. Chem.*, 2015, p. 1958.

52. Sarria, O.A., Basiuk, V.A., Alaniz, V.D., and Rivera, M., *Phys. Chem. Chem. Phys.*, 2015, vol. 17, p. 27399.

53. Khavasi, H.R. and Sadegh, B.M.M., *Dalton Trans.*, 2014, vol. 43, p. 5564.

54. Qian, X., Johnson, D.K., Himmel, M.E., and Nimlos, M.R., *Carbohydrate Res.*, 2010, vol. 345, p. 1945.

55. Saha, S., Sasmal, A., Choudhury, C.R., et al., *Inorg. Chim. Acta*, 2015, vol. 425, p. 211.

56. Tsuzuki, S., Honda, K., Uchimaru, T., et al., *J. Phys. Chem., A*, 2006, vol. 110, p. 10163.

57. Tsuzuki, S. and Fujii, A., *Phys. Chem. Chem. Phys.*, 2008, vol. 10, p. 2584.

58. Kumar, M., Sheikh, H.N., Fraconetti, A., et al., *New J. Chem.*, 2019, vol. 43, p. 2179.

59. Roselló, Y., Benito, M., Bagués, N., et al., *Cryst. Growth Des.*, 2020, vol. 20, p. 2985.